Title page

Spatiotemporal distribution of the extracellular matrix changes during mouse duodenojejunal flexure formation

Sawa Onouchi[1], Osamu Ichii[1], Teppei Nakamura[1, 2], Yaser Hosny Ali Elewa[1, 3], Yasuhiro Kon[1*]

[1]Laboratory of Anatomy, Department of Biomedical Sciences, Graduate School of Veterinary Medicine, Hokkaido University, Sapporo, Hokkaido, Japan

[2]Section of Biological Safety Research, Chitose Laboratory, Japan Food Research Laboratories, Chitose, Hokkaido, Japan

[3]Department of Histology and Cytology, Faculty of Veterinary Medicine, Zagazig University, Zagazig, Egypt

[*]Corresponding author:

Yasuhiro Kon, DVM, PhD,

Laboratory of Anatomy, Department of Biomedical Sciences,

1 Graduate School of Veterinary Medicine,

2 Hokkaido University, Kita 18, Nishi 9, Kita-ku,

3 Sapporo 060-0818, Japan

4 Tel/Fax: 011-706-5189;

5 E-mail: y-kon@vetmed.hokudai.ac.jp

6

7

Abstract

Although gut flexures characterize the gut morphology, the mechanisms underlying flexure formation remain obscure. Previously, we analyzed the mouse duodenojejunal flexure (DJF) as a model for its formation, and reported asymmetric morphologies between the inner and outer bending sides of the fetal mouse DJF, implicating their contribution to DJF formation. In this study, we present the extracellular matrix (ECM) as an important factor for gut morphogenesis. We investigated the ECM distribution during mouse DJF formation using histological techniques. In the intercellular space of the gut wall, high Alcian Blue-positivity, for proteoglycans, shifted from the outer to the inner side of the gut wall during DJF formation. However, the immunopositivity for fibronectin-, collagen I-, or pan-tenascin was higher at the inner, than at the outer side. Further, collagen IV and laminins localized to the epithelial basement membrane. Beneath the mesothelium at the pre-formation stage, collagen IV and laminin immunopositivity showed inverse results, corresponding to the difference in cellular characteristics at this site. At the post-formation stage, however, laminin-positivity beneath the mesothelium was the reverse of that observed during the pre-formation stage. In addition, high immunopositivity for collagen IV and laminins at the inner gut wall mesenchyme of post-formation DJF implied different blood vessel distribution. Therefore, we concluded that

ECM distribution changes spatiotemporally during mouse DJF formation, thus indicating its association with the establishment of asymmetric morphologies during DJF formation.

Keywords: Gut morphogenesis, Flexure formation, Extracellular matrix, Duodenojejunal flexure

Introduction

During gut morphogenesis, the gut tube acquires asymmetric features through gut rotation and looping. Gut looping is important for the formation of gut flexures, required for compaction of the long gut tube to fit into the abdominal cavity. A recent study in chicks and mice reported that gut looping in the jejunum occurs due to differences in elongation rates of the gut tube and its dorsal mesentery (Savin et al. 2011).

In contrast, the mouse duodenojejunal flexure (DJF), located between the duodenum and jejunum, is formed in the midgut from embryonic day (E)10.75 to E11.75. This is independent of the umbilical hernia, where abundant flexures are generated by the asymmetric degree of the elongation between the gut tube and its mesentery. We previously reported that the dorsal mesentery has little connection with mouse DJF formation, and presented the DJF as a model for flexure formation, formed by the gut original power (Onouchi et al. 2013). We also reported the following observations about morphological changes in the DJF (Onouchi et al. 2013, 2015). First, at around E10.75, the region where the DJF forms appeared expanded, without a flexure. At E11.25–E11.75, this region exhibited flexure formation along the dorsal-ventral axis. Subsequently, the flexure elongated towards the left and cranial directions in the abdominal cavity, as it surrounded the stomach. Previous studies also reported asymmetric gene expression of the hedgehog and retinoid signaling pathways during DJF formation, as well as asymmetric

morphologies, such as cell proliferation, cell polarity, and neural cell differentiation, between the inner and outer bending sides of the mouse DJF (Onouchi et al. 2013, 2015). The hedgehog and retinoid signaling pathways control cell proliferation and differentiation (Mao et al. 2010; Gutierrez-Mazariegos et al. 2011), and asymmetric morphology plays a crucial role in organ morphogenesis, such as that of the stomach and heart (Taber 2006; Burn and Hill 2009). Therefore, we hypothesized that mouse DJF formation is due to such asymmetric morphologies, controlled by the expression of genes involved in signaling pathways.

The extracellular matrix (ECM) is a component of the connective tissues and fibers, excluding cells. The ECM plays an important role, not only in structural support, but also in the control of cellular behavior such as survival, proliferation, differentiation, polarity, and migration (Hynes 2009). During cell proliferation, several proteoglycans that contain heparin and heparan sulfate act as reservoirs of growth factors, such as fibroblast growth factors (FGF), transforming growth factor-β (TGF-β), bone morphogenetic proteins, and sonic hedgehog. Moreover, the distribution of proteoglycans provides growth factor gradients for patterning during development (Hynes 2009). These proteoglycans are also required for ligand reception and signal activation by FGF and TGF-β (Hynes 2009; Shimokawa et al. 2011). In addition, ECM receptors, including integrins, acts as signal transducers, thus playing important roles in regulating cell behavior (Kim et al. 2011; Legate et al. 2009). Briefly, once ECM molecules

connect to these receptors, the receptors activate several intracellular signaling pathways for cell proliferation, cell survival, cell shaping, and cell migration. Moreover, there exists a crosstalk between these ECM receptors and growth factor receptors which activate intracellular signaling pathways similar to those pathways that act the downstream of integrins (Kim et al. 2011; Legate et al. 2009). Given our observations about asymmetric morphology, we addressed the relationship between the ECM and asymmetric morphology during DJF formation in this study.

Here, we investigated the distributions of typical ECM molecules, including proteoglycans, fibronectin, collagen I and IV, tenascin, and laminin, in developing mouse DJF. We compared their distributions at the inner and outer bending sides of the DJF. Our results suggest that all of the studies ECM molecules were asymmetrically distributed at either the pre- or post-formation stage of the DJF. Therefore, we present an important relationship between ECM molecules and DJF formation.

Materials and methods

Animals and sample preparation

Pregnant C57BL/6 mice were purchased from Japan SLC, Inc. (Shizuoka, Japan). Noon on the day that a vaginal plug was found was designated E0.5. These mice were sacrificed, and embryos at age E10.75 (pre-formation stage) and E11.5–E11.75 (post-formation stage) were used for subsequent analyses. Whole embryos and dissected gut tubes were used at the pre- and post-formation stages, respectively. These tissues were fixed overnight with 4% paraformaldehyde (PFA) in 0.1 M phosphate buffer (pH 7.4) at 4°C, and embedded in 1% agarose prior to embedding in paraffin in order to ensure the precise angle and face of slicing. The mice were handled in accordance with the Guide for the Care and Use of Laboratory Animals of Hokkaido University, Graduate School of Veterinary Medicine (approved by the Association for Assessment and Accreditation of Laboratory Animal Care International).

Alcian Blue staining for proteoglycan detection

Cross- and sagittal-sections (semi-serial, 3-μm-thick) of gut tubes were prepared at the pre- and post-formation stages, respectively. The sections were deparaffinized and stained with pH1.0 and pH2.5 Alcian Blue. Alcian Blue staining at pH1.0 detects proteoglycans containing sulfate groups, while that at pH2.5 detects proteoglycans primarily containing carboxyl groups, along

with sulfate groups. Briefly, following incubation with either 1N HCl (pH1.0) or 3% acetic acid (pH2.5) for 3 min, the sections were treated with 1% Alcian Blue regent (either pH1.0 or pH2.5). Next, the sections were washed with either 100% ethanol (pH1.0) or 3% acetic acid (pH2.5) for 5 min. At the pre-formation stage, the DJF was defined as the region located at the caudal position of the pancreatic buds and attached to the dorsal and ventral mesenteries (Onouchi et al. 2013). At the post-formation stage, we selected gut sections that showed a clear and distinct lumen. To confirm the identity of the Alcian Blue stained area, we counterstained selected sections with eosin at the post-formation stage, after Alcian Blue staining, by treating the sections with eosin regent for 1 sec (pH 1.0) or 10 sec (pH2.5).

Immunohistochemistry for ECM molecules and blood vessels markers

To determine the distribution of each ECM molecule, at the pre- and post-formation stages, we performed immunohistochemistry for fibronectin, collagen I, pan-tenascin, collagen IV, pan-laminin, and laminin 1/2. In addition, we performed immunohistochemistry for the blood vessel markers, CD31 and CD34, at the post-formation stage. The details of the staining conditions and primary antibodies are described in Table 1. Briefly, either the cross- or sagittal-sections (semi-serial, 3-μm-thick) were deparaffinized, heated, and treated with primary and secondary antibodies according to a previously published streptavidin-biotin method

(Onouchi et al. 2013). The color was developed by incubating in 3,3′-diaminobenzidine tetrahydrochloride (DAB)-H_2O_2 solution. In this study, “pan-tenascin” indicates all members of the tenascin family (tenascin C/R/W/X), “pan-laminin” indicates all laminin isoforms, and “laminin 1, 2” indicates laminin 1 (α1, β1, γ1) and 2 (α2, β1, γ1) isoforms.

Immunofluorescent detection of N-cadherin

DJF sections at the pre-formation and the post-formation stage (semi-serial, 3-μm-thick) were deparaffinized and heated with citrate buffer, pH6.0. After blocking, the sections were treated with primary antibodies against N-cadherin, and then with Alexa Fluor 546-labeled secondary antibodies.

Histoplanimetrical analysis of ECM distribution

For analysis of ECM distribution in the gut wall, Alcian Blue-stained and immunohistochemical sections were used for histoplanimetry (Fig. 1). Semi-serial cross- and sagittal-sections were used at the pre- and post-formation stages, respectively. The integrated densities (IntDen) of Alcian Blue- and immune-positivity were quantified using the ImageJ software (National Institutes of Health; Bethesda, MD, USA). IntDen refers to the sum of signal intensities over a defined area. Because the signal was not immediately clear, digital images

were processed as follows. We drew boundaries between the inner and outer bending sides of the DJF on digital images (Fig. 1). At the pre-formation stage, we defined the inner and outer areas as the left and right areas of the DJF gut wall, not including the mucosal epithelium, divided by a straight line crossing the dorsal and ventral mesenteries, respectively (Fig. 1a). At the post-formation stage, we placed a 100 μm square area around the center of the top of the DJF and defined the boundary between the inner and outer bending sides of the DJF as the mucosal epithelium (Fig. 1b). In order to highlight the signal, we reduced the background color by using Photoshop (Adobe Systems Incorporated; San Jose, CA, USA). After that, we converted RGB color images into black and white, and subsequently switched the signal color from black to white. Finally, we analyzed IntDen for the signal on the processed images using ImageJ.

To easily detect the differences between the inner and outer bending sides, we calculated their respective IntDen ratios in the following manner: the IntDen of the inner side divided by itself (IntDen ratio of the inner side); the IntDen of the outer side divided by the IntDen of the inner side (IntDen ratio of the outer side). Therefore, the value of the IntDen ratio of the inner side was always equal to 1.0, and we could easily calculate the differences as the relative changes in the value of the outer side.

At the pre-formation stage, the IntDen ratios for stain-positive reactions were compared

between the separated left and right halves, corresponding to the inner and outer areas, respectively, of the gut wall (Fig. 1a). During the development from the pre-formation to post-formation stage, the DJF rotates counterclockwise around the cranio-caudal gut axis, at approximately 90°, to bend the left and right sides of the DJF along the dorsal-ventral axis (Onouchi et al. 2013). Therefore, at the pre-formation stage, the left and right sides of the DJF were analyzed. At the post-formation stage, the area analyzed was either the inner or outer gut wall, located in the range of 100 μm from the center of the top of the DJF (Fig. 1b). For analyses at both stages, the average IntDen of three sections from each embryo was considered an individual value, which was used for calculating the individual IntDen ratio as described above. The average of the IntDen ratios for more than four specimens was compared between the inner and outer bending sides of the DJF.

For the ECM molecules located at the epithelial basement membrane (collagen IV, pan-laminin, laminin 1/2); in particular, the IntDens for immuno-positive reactions were measured separately on the outside and inside areas. Briefly, we defined the boundary between the two areas as the line drawn 25 μm below the surface of the DJF at the pre-formation and post-formation stages (Fig. 1). Therefore, the outside area included both the mesothelial and endothelial basement membranes beneath the mesothelium, while the inside area included the mucosal epithelial and endothelial basement membrane.

Statistical analysis

Results are expressed as the mean ± standard error (SE). For statistical differences between the inner and outer bending sides of the DJF, a nonparametric Wilcoxon test ($P < 0.05$) was performed.

Results

Distribution of proteoglycans at the pre- and post-formation stages.

In order to detect proteoglycans containing sulfate and carboxyl groups, Alcian Blue staining at pH1.0 and pH2.5, respectively, was performed at the pre- and post-formation stage DJFs (Fig. 2). In the gut tube, Alcian Blue-positivity at both pH values was detected around the gut wall cells, but not within their cytoplasm or nuclei (Fig. 2a-d). Alcian Blue-positivity at pH1.0 was detected mainly in the intercellular spaces as well as epithelial basement membrane of the gut wall at both stages (Fig. 2e and f; daggers, arrowheads, and arrows). Meanwhile, Alcian Blue-positivity at pH2.5 was detected only in the intercellular spaces of the gut wall at both stages (Fig. 2h and i; daggers). At the pre-formation stage, the IntDen ratios of positive reactions were higher at the outer side of the DJF than at the inner side, for both pH1.0 (Fig. 2g) and pH2.5 (Fig. 2j); a significant difference was observed for the latter. However, the IntDen ratios for both stain-positive reactions were significantly higher at the inner side of the DJF than at the outer side at the post-formation stage (Fig. 2g and j).

Distribution of fibronectin and collagen I at the pre- and post-formation stages.

To detect other ECM molecules, immunohistochemistry was performed at the pre- and post-formation stage DJFs. At both stages, fibronectin-positivity was detected at the intercellular

spaces of the whole-gut wall and the mucosal epithelial basement membrane (Fig. 3a and b; daggers, and arrows). The IntDen ratio for fibronectin-positivity was significantly higher at the inner side of the DJF than at the outer side at the post-formation, but not pre-formation stage (Fig. 3c).

Collagen I-positivity was detected in part of the intercellular spaces in the gut wall of the DJF (Fig. 3d, e, g; arrowheads). The reaction intensities were weaker than that for the other ECM molecules examined. At the pre-formation stage, the reactions were limited to the gut wall, close to the dorsal and ventral mesenteries (Fig. 3d; black arrowheads). Further, the IntDen ratio for collagen I-positivity was not different between the inner and outer bending sides of the DJF (Fig. 3f). However, at the post-formation stage, the reactions were much stronger at the outside of the gut wall at the inner side of the DJF (Fig. 3e and g). Some reactions appeared to be distributed along a line, similar to the basement membrane (Fig. 3g; white arrowheads). The IntDen ratio for collagen I-positivity was significantly higher at the inner side of the DJF than at the outer side at the post-formation stage (Fig. 3e and f).

Distribution of pan-tenascin at the pre- and post-formation stages.

At the pre-formation stage, pan-tenascin-positivity was broadly detected at the intercellular spaces from the mesothelial to the mucosal epithelial basement membranes in the

inner side of the DJF (Fig. 4a and d). In particular, the reactions at the intercellular spaces close to the mesothelial basement membrane (Fig. 4d) tended to be stronger than those at the intercellular spaces close to the mucosal epithelial basement membrane (Fig. 4a; arrowhead). Strong positive reactions were also detected at the dorsal mesentery (Fig. 4a; DM). The IntDen ratio for pan-tenascin-positivity was significantly higher at the inner side of the DJF than at the outer side at the pre-formation stage (Fig. 4c). However, at the post-formation stage, it was only faintly detected at the intercellular spaces of the outside gut wall at the inner and outer bending sides of the DJF (Fig. 4b; arrowheads). The dorsal mesentery, meanwhile, maintained its pan-tenascin-positivity (Fig. 4b; DM). Further, the IntDen ratio for pan-tenascin-positivity did not differ between the inner and outer sides of the DJF at the post-formation stage (Fig. 4c).

Distribution of collagen IV at the pre- and post-formation stages.

Next, in order to examine the basement membrane, we used immunohistochemistry to detect collagen IV and laminins (Fig. 5 and 6). We independently measured the IntDen ratios at the inside area for the mucosal epithelial and endothelial basement membranes, and at the outside area for the mesothelial and endothelial basement membrane beneath the mesothelium (see Fig. 1). Collagen IV-positivity was detected mainly in the mucosal epithelial and endothelial basement membranes at both stages (Fig. 5a, b, f; arrowheads), partly in the mesothelial

basement membrane of the DJF at the pre-formation stage, but rarely at the post-formation stage (Fig. 5a, b, d, e; arrows). At the pre-formation stage, the collagen IV-positivity in the mesothelial basement membrane was stronger and more assembled at the inner, than at the outer side of the DJF (Fig. 5d and e). Therefore, the IntDen ratio for collagen IV-positivity in the outside area was significantly higher at the inner side of the DJF than at the outer side; however, that for the inside area did not differ at the pre-formation stage (Fig. 5c). On the other hand, at the post-formation stage, the IntDen ratio for the outside area was not significantly different between the inner and outer sides of the DJF (Fig. 5c), while that for the inside area was significantly higher at the inner, than at the outer side of the post-formation stage DJF (Fig. 5c).

Distribution of pan-laminin- and laminin 1/2 at the pre- and post-formation stages.

Pan-laminin-positivity was detected in the mucosal epithelial, endothelial, (Fig. 6a, d, g; arrowheads) and mesothelial (Fig. 6a–f, arrows) basement membranes in the DJF at the pre- and post-formation stages. Compared with collagen IV-positivity, the pan-laminin-positive reactions in the mesothelial basement membrane, in particular at the pre-formation stage, was broader and more scattered (Fig. 5a, d, e, 6a–c). At the pre-formation stage (Fig. 6a), the IntDen ratios for pan-laminin-positivity in both the outside and inside areas were significantly higher at the outer side of the DJF than at the inner side (Fig. 6b, c, h). On the other hand, at the post-formation

stage (Fig. 6d), the IntDen ratios for both the outside and inside areas were significantly higher at the inner side of the DJF than at the outer side (Fig. 6e, f, h). Since the inside area mainly contains the endothelial basement membrane along with blood vessels in the gut wall, we performed immunohistochemistry for CD31, a blood vessel marker, at the post-formation stage (Fig. S1a). This yielded a significantly higher IntDen ratio for the inner side, than for the outer side of the DJF (Fig. S1c).

Meanwhile, laminin 1/2-positivity was detected in the mucosal epithelial (Fig. 7a and d; arrowheads) and mesothelial (Fig. 7a–f; arrows) basement membranes. Additionally, it was either absent or present in low amounts in the endothelial basement membrane, in the DJF at the pre- and post-formation stages. At the pre-formation stage, laminin 1/2 positivity in the mesothelial basement membrane appeared as a line, and assembled at the inner side, while being broadly scattered at the outer side (Fig. 7b and c). The IntDen ratio for laminin 1/2-positivity in the outside area was significantly higher at the outer side of the DJF than at the inner side, similar to that for the pan-laminin-positive reactions (Fig. 7g). However, at the post-formation stage, laminin 1/2-positivity in the mesothelial basement membrane was weaker and appeared scattered in both the sides (Fig. 7e and f). The IntDen ratios for both the outside and inside areas did not differ between the inner and outer sides of the post-formation stage DJF. This was not similar to the IntDen ratio for the pan-laminin-positive reactions (Fig. 7g).

Since significant differences were observed for the IntDen ratios for all the basement membrane ECM molecules at the outside area of the pre-formation stage DJF, we hypothesized that the morphological property of the cell in the outside area differs from that in the inside area. To test this, immunohistochemistry for N-cadherin, an adhesion molecule, was performed at the pre-formation stage DJF (Fig. 7h–j). Although N-cadherin-positivity was detected at the most of mesenchymal cells, the results indicated strong N-cadherin-positivity in several cells surrounding the mucosal epithelium, which were neural crest cells and neurons as described in our previous study (Onouchi et al. 2015; Fig. 7h; arrowheads). In addition, the mesothelium in both the dorsal mesentery and the outside area of the gut wall extending from the dorsal mesentery was N-cadherin-positive (Fig. 7i and j). N-cadherin-positivity in the outside area surrounded the mesothelial cells, in particular at the inner side, while that at the outer side was weak (Fig. 7i and j; arrows). On the other hand, we did not detect clear difference beneath the mesothelium between the inner and outer bending sides in the post-formation stage DJF, stained with N-cadherin antibodies (Fig. 7k–m).

Discussion

In this study, we demonstrated asymmetric distributions of several ECM molecules during DJF formation, as summarized in Figure 8 and Table 2.

In our results, Alcian Blue-positivity at the pre- and post-formation stages was stronger at the outer and inner side of the DJF, respectively, than at the opposite side at both pH1.0 and pH2.5. Alcian Blue staining detects proteoglycans, which are made of a core protein containing several types of glycosaminoglycan chains. Glycosaminoglycans are roughly divided into chondroitin sulfate, heparan sulfate, dermatan sulfate, and keratan sulfate. These glycosaminoglycan chains have abundant sulfate groups and carboxyl groups that stain blue with Alcian Blue. Recent studies reported that some heparan sulfate proteoglycans, such as syndecan, control the localization of several growth factors and modify their activities and reception in mammals (Hynes 2009; Shimokawa et al. 2011; Iozzo and Schaefer 2015). However, we previously reported higher cell proliferation rates at the outer side of the DJF than at the inner at the post-formation, but not pre-formation stage (Onouchi et al. 2013). There are many kinds of proteoglycans, which play different roles, even within the heparan sulfate proteoglycan group. For example, perlecan is known as a regulator of angiogenesis (Iozzo and Schaefer 2015). Unfortunately, investigating each proteoglycan component with Alcian Blue was beyond the scope of this study. However, we demonstrated that the distribution of

proteoglycans alters during DJF formation.

Fibronectin- and collagen I-positivity were higher at the inner side of the DJF than at the outer side at the post-formation stage, suggesting the abundance of these ECM molecules. Fibronectin is a large glycoprotein ubiquitously expressed throughout the body. An important property of fibronectin is its ability to bind to other ECM molecules and to integrin receptors on the cell surface (Labat-Robert 2012). On the other hand, collagen I is a fibril-forming collagen that is abundantly expressed in interstitial tissues including bones, tendon, ligaments, and dermis. Collagen I provides structural stiffness for the tissue and helps it to resist tensile and torsional stresses (Gelse et al. 2003). In addition, collagen I is also recognized by integrins (Leitinger 2011), which are components of focal adhesion for cell-ECM interactions. Integrins sense mechanical force originating from the ECM and mediate several intracellular signals to control the actin cytoskeleton for cell morphology and migration (Geiger et al. 2009; Janoštiak et al. 2014). Recent studies have indicated that ECM rigidity is sensed by integrins to guide cell migration toward stiff ECM (Plotnikov et al. 2012). Since we detected more abundant distribution of fibronectin and collagen I at the inner side of the DJF than at the outer side, we hypothesized that the inner side had comparatively stiffer ECM. In addition, we reported that the gut wall of the inner side was thicker than that of the outer side of the DJF, suggesting more abundant cells at the inner side (Onouchi et al. 2013). Therefore, fibronectin and collagen I at

the inner side might contribute to the accumulation of gut wall cells, leading to different elongation rates between the inner and outer sides for DJF bending.

The pan-tenascin-positive reactions were higher at the inner side of the DJF than at the outer at the pre-formation stage. The tenascin family includes 4 members: tenascin C, R, W, and X. These proteins are well known for their ability to modulate cell adhesion and migration (Chiquet-Ehrismann and Tucker 2011). Tenascin C is the most studied member because of its spatiotemporal expression during embryogenesis. Recent reports suggest that tenascin C performs several functions including cell proliferation, apoptosis, and differentiation in addition to controlling cell migration (Jones and Jones 2000). Therefore, we proposed that pan-tenascin affects gut wall cells in the DJF because of its ability to modulate cell migration. Notably, the effect of tenascins, in particular tenascin C, depends on the cell type, species, and context (Jones and Jones 2000; Breau et al. 2009; Akbareian et al. 2013). Therefore, we hypothesized that tenascin C expression at the inner side of the DJF at the pre-formation stage is necessary for accumulation of gut wall cells in the same, through the control of cell migration.

Immuno-positivity for collagen IV, pan-laminin, and laminin 1/2, ECM molecules that make up the epithelial basement membranes, was also detected. Collagen IV is a member of the collagen family and expressed only in the basement membranes. It is a heterotrimer composed of a combination of six α-chains: α1α1α2, α3α4α5, and α5α5α6 (Khoshnoodi et al. 2008).

Laminins are also chief components of the epithelial basement membrane, and are heterotrimeric proteins composed of α, β, and γ chains. Since each chain has multiple variants, laminins are divided into more than 15 isoforms depending on the combination of the 3 chains (Hohenester and Yurchenco 2013). This study revealed remarkable differences in the IntDen ratios between the inner and outer bending sides of the DJF in the basement membranes located in the outside area, including mainly the mesothelial basement membrane. Interestingly, at the pre-formation stage, the IntDen ratios for collagen IV- and laminins-positivity showed opposite results, suggesting that the components of the basement membrane are different between the inner and outer bending sides of the pre-formation stage DJF. In addition, the IntDen ratio for laminin 1/2-positivity at the pre-formation stage was similar to that of the pan-laminin-positive reactions. Therefore, the difference in pan-laminin-positivity in the outside area is partially caused by the difference in the distribution of laminin 1 or laminin 2. Laminin 1 is expressed in the mucosal epithelial basement membrane in the early stages of the developing rat intestine, while laminin 2 is expressed around birth (Simon-Assmann et al. 1998). Therefore, we suggest that the laminin isotype that the laminin 1/2 antibody detected in this study was laminin 1. Interestingly, our previous study showed that cell size in the outside area was significantly different between the inner and outer bending sides of the DJF. Based on this, we considered the possibility of a difference in cell polarity between the two sides (Onouchi et al. 2013).

Further, this study revealed differences in the adhesive property, as indicated by N-cadherin expression, in cells in the outside area. During gut morphogenesis, laminin 1 is important for the polarization of epithelial cells as well as for cell differentiation (De Alcangelis et al. 1996). Collagen IV is important for basement membrane stability (Pöschl et al. 2003), though there are only few reports on the involvement of collagen IV in morphogenesis. Therefore, we proposed that the difference in collagen IV-positivity is related to cell morphology, including polarization, and properties of the outside cells at the pre-formation stage.

On the other hand, at the post-formation stage, the IntDen ratio for pan-laminin was higher at the inner side of the DJF than at the outer side, which was not similar to that for the laminin 1/2-positive reactions. We also proposed that the laminin isoforms abundantly expressed at the inner side at the post-formation stage are different from laminin 1 and 2, suggesting that the components of the basement membrane changed during DJF formation. This was supported by the observation that laminin 1/2-positivity in the outside area decreased at the post-formation stage. In addition, in the inside area of the post-formation stage DJF, the IntDen ratios for collagen IV- and pan-laminin-positivity were higher at the inner side, than at the outer side. We hypothesized that this difference was due to the difference in vascular distribution. We reported that vascular distribution detected by CD34 antibodies was same in both the sides

(Onouchi et al. 2015). However, the IntDen ratio for CD31-positivity, another vascular marker, was significantly higher at the inner side, than at the outer side at the post-formation stage in this study. The section stained by CD34 antibodies showed considerable background staining because of CD34 expression in other cells including vascular endothelial progenitor cells, embryonic fibroblasts, and multipotent mesenchymal stromal cells (Sidney et al. 2014). The vessels stained more weakly than did the section stained by CD31 (Fig. S1a and b). This affected the differences between IntDen ratios for the CD34- and CD31-positive reactions.

For the basement membrane comprising ECM, the components located in the outside area were different at the inner and outer bending sides of the DJF, at least at the pre-formation stage, and changed during DJF formation. Our previous study also showed significant differences in cell morphology in the outside area at the pre- and post-formation stages (Onouchi et al. 2013). Therefore, a change in composition of the basement membrane located in the outside area might be associated with outside cell morphology.

Although we detected distinct patterns of ECM distribution, further studies are needed to identify the factors that form these patterns. We assume that asymmetric synthesis or degradation of ECM molecules determine the patterns of ECM distribution. Recently, factors contributing to ECM metabolism have been slowly uncovered. TGF-β, a ubiquitous cytokine produced by every cell, promotes ECM secretion through its type II receptor. In an adult mouse

gut, the type II receptor is expressed on smooth muscle cells, fibroblasts, and myofibroblasts. In addition, the population of the fibroblasts and myofibroblasts increase during inflammation, and these cells secrete collagen I, collagen IV, and laminin (Whiting et al. 2003). Therefore, TGF-β may be one of the factors that contribute to asymmetric ECM distribution. Moreover, matrix metalloproteinases (MMPs) are key enzymes for ECM degradation. During chick cardiac looping, ECM asymmetry in the dorsal mesocardium defines the looping direction. This asymmetry appears to be achieved by asymmetric MMP inhibition (Linask et al. 2005). Therefore, MMPs are also candidate factors. In future experiments, we will identify critical factors for asymmetric ECM distribution.

The DJF rotates counter clockwise around the cranio-caudal gut axis to bend the left and right sides of the DJF along the dorsal-ventral axis (Onouchi et al. 2013). Therefore, DJF formation is ideally a left-right asymmetric phenomenon. In gut development, the left-right asymmetric morphology in the dorsal mesentery determines the direction of gut rotation (Davis et al. 2008; Welsh et al. 2013). Interestingly, we found that several morphological asymmetries in the DJF were similar to those in the dorsal mesentery (Onouchi et al. 2013; 2015). Moreover, asymmetric ECM distribution also occurs in the dorsal mesentery (Kurpios et al. 2008). In the dorsal mesentery, such asymmetries are formed by the family of transcription factors known as the downstream of left identity, such as paired-like homeodomain transcription factor 2 (known

as Pitx2) (Davis et al. 2008; Kurpios et al. 2008; Welsh et al. 2013). Therefore, DJF formation may also be controlled by those transcription factors related to left-right axis formation.

In conclusion, ECM distribution is different between the inner and outer bending sides of the DJF, and this distribution changes during DJF formation.

Acknowledgments

This work was supported by the JSPS KAKENHI (grant numbers 2600167304). The research described in this paper was selected for the Encouragement Award at the 158th Japanese Association of Veterinary Anatomists in Aomori (September 7–9, 2015). We would like to thank all the people involved.

Table 1 Antibodies and conditions used in this study for immunohistochemistry

Target	Primary Antibody	Antigen Retrieval	Dilution	Secondary Antibody
Collagen I	Rabbit polyclonal antibodies (Abcam, Cambridge, UK)	Citrate buffer solution, pH6.0, 105°C, 20 min	1:1,000	Biotinylated goat anti-rabbit IgG antibodies (SABRO kit; Nichirei)
Collagen IV	Rabbit polyclonal antibodies (Abcam)	Citrate buffer solution, pH6.0, 105°C, 20 min	1:10,000	Biotinylated goat anti-rabbit IgG antibodies (SABRO kit; Nichirei)
Fibronectin	Rabbit polyclonal antibodies (Abcam)	Citrate buffer solution, pH6.0, 105°C, 20 min	1:10,000	Biotinylated goat anti-rabbit IgG antibodies (SABRO kit; Nichirei)
Pan-laminin	Rabbit polyclonal antibodies (Sigma-Aldrich,	—	1:200	Biotinylated goat anti-rabbit IgG antibodies (SABRO kit; Nichirei)

	Saint Louis, MO, USA)			
Laminin 1/2	Rabbit polyclonal antibodies (Novus Biologicals, Littleton, CO, USA)	Citrate buffer solution, pH6.0, 105℃, 20 min	1:10,000	Biotinylated goat anti-rabbit IgG antibodies (SABRO kit; Nichirei)
Pan-tenascin	Rat monoclonal antibodies (Sigma-Aldrich)	Tris-HCl buffer solution, pH9.0, 105℃, 20 min	1:10,000	Biotinylated goat anti-rat IgG antibodies
CD31	Rabbit polyclonal antibodies (Abcam)	Tris-HCl buffer solution, pH9.0, 105℃, 20 min	1:100	Biotinylated goat anti-rabbit IgG antibodies (SABRO kit; Nichirei)
CD34	Rat monoclonal	Citrate buffer	1:400	Biotinylated goat anti-rat

	antibodies (Abcam)	solution, pH6.0, 105°C, 20 min		IgG antibodies
N-cadherin	Rabbit polyclonal antibodies (Abcam)	Citrate buffer solution, pH6.0, 105°C, 20 min	1:2,000	Alexa fluor 546-labeled donkey anti-rabbit IgG antibodies (Life Technologies, Waltham, MA, USA)

Table 2 Summary of distribution of the ECM molecules studied in the mouse duodenojejunal flexure (DJF)

*< and > indicate the side with higher IntDen ratio between the inner and outer bending sides of the DJF. AB, Alcian Blue.

ECM molecules	Pre-formation*	Post-formation*
pH1.0 AB	−	Inner > Outer
pH2.5 AB	Inner < Outer	Inner > Outer
Fibronectin	−	Inner > Outer
Collagen I	−	Inner > Outer

Pan-tenascin	Inner > Outer	−
Collagen IV	Inner > Outer at outside	Inner > Outer at inside
Pan-laminin	Inner < Outer	Inner > Outer
Laminin 1/2	Inner < Outer at outside	−

1

References

- Akbareian SE, Nagy N, Steiger CE, Mably JD, Miller SA, Hotta R, Molnar D, Goldstein AM (2013) Enteric neural crest-derived cells promote their migration by modifying their microenvironment through tenascin-C production. Dev Biol 382:446-456
- Breau MA, Dahmani A, Broders-Bondon F, Thiery JP, Dufour S (2009) β1 integrins are required for the invasion of the caecum and proximal hindgut by enteric neural crest cells. Development 136:2791-2801
- Burn SF, Hill RE (2009) Left-right asymmetry in gut development: what happens next? BioEssays 31:1026–1037
- Davis NM, Kurpios NA, Sun X, Gros J, Martin JF, Tabin CJ (2008) The chirality of gut rotation derives from left-right asymmetric changes in the architecture of the dorsal mesentery. Dev Cell 15:134–145
- De Arcangelis A, Neuville P, Boukamel R, Lefebvre O, Kedinger M, Simon-Assmann P (1996) Inhibition of Laminin α1-chain expression leads to alteration of basement membrane assembly and cell differentiation. J Cell Biol 133:417-430
- Gelse K, Pöschl E, Aigner T (2003) Collagens—structure, function, and biosynthesis. Adv Drug Deliv Rev 55:1531-1546
- Gutierrez-Mazariegos J, Theodosiou M, Campo-Paysaa F, Schubert M (2011) Vitamin A: a

multifunctional tool for development. Semin Cell Dev Biol 22:603–610

· Geiger B, Spatz JP, Bershadsky AD (2009) Environmental sensing through focal adhesions. Nat Rev Mol Cell Biol 10:21–33

· Hohenester E, Yurchenco PD (2013) Laminins in basement membrane assembly. Cell Adh Miqr 7:56–63

· Hynes RO (2009) The extracellular matrix: not just pretty fibrils. Science 326:1216–1219

· Iozzo RV, Schaefer L (2015) Proteoglycan form and function: A comprehensive nomenclature of proteoglycans. Matrix Biol 42:11–55

· Janoštiak R, Pataki AC, Brábek J, Rösel D (2014) Mechanosensors in integrin signaling: the emerging role of p130Cas. Eur J Cell Biol 93:445–454

· Jones FS, Jones PL (2000) The tenascin family of ECM glycoproteins: structure, function, and regulation during embryonic development and tissue remodeling. Dev Dyn 218:235–259

· Khoshnoodi K, Pedchenko V, Hudson BG (2008) Mammalian Collagen IV. Microsc Res Tech 71:357–370

· Kim SH, Turnbull J, Guimond S (2011) Extracellular matrix and cell signaling: the dynamic cooperation of integrin, proteoglycan and growth factor receptor. J Endocrinol 209:139–151

- Kurpios NA, Ibañes M, Davis NM, Lui W, Katz T, Martin JF, Izpisúa Belmonte JC and Tabin CJ (2008) The direction of gut looping is established by changes in the extracellular matrix and in cell: cell adhesion. Proc Natl Acad Sci USA. 105: 8499-8506
- Labat-Robert J (2012) Cell-Matrix interactions, the role of fibronectin and integrins. A survey. Pathol Biol 60:15–19
- Legate KR, Wickström SA, Fässler R (2009) Genetic and cell biological analysis of integrin outside-in signaling. Genes Dev 23:397–418
- Leitinger B (2011) Transmembrane collagen receptors. Annu Rev Cell Dev Biol 27:265–290
- Linask KK, Han M, Cai DH, Brauer PR, Maisastry SM (2005) Cardiac morphogenesis: matrix metalloproteinase coordination of cellular mechanisms underlying heart tube formation and directionality of looping. Dev Dyn 233:739-753
- Mao J, Kim BM, Rajurkar M, Shivdasani RA, McMahon AP (2010) Hedgehog signaling controls mesenchymal growth in the developing mammalian digestive tract. Development 137:1721–1729
- Onouchi S, Ichii O, Otsuka S, Hashimoto Y, Kon Y (2013) Analysis of duodenojejunal flexure formation in mice: implications for understanding the genetic basis for gastrointestinal morphology in mammals. J Anat 223:385–398

- Onouchi S, Ichii O, Kon Y (2015) Asymmetric morphology of the cells comprising the inner and outer bending sides of the murine duodenojejunal flexure. Cell Tissue Res 360:273–85
- Plotnikov SV, Pasapera AM, Sabass B, Waterman CM (2012) Force fluctuations within focal adhesions mediate ECM-rigidity sensing to guide directed cell migration. Cell 151:1513–1527
- Pöschl E, Schlötzer-ZSchrehardt U, Brachvogel B, Saito K, Ninomiya Y, Mayer U (2003) Collagen IV is essential for basement membrane stability but dispensable for initiation of its assembly during early development. Development 131:1619–1628
- Savin T, Kurpios NA, Shyer AE, Florescu P, Liang H, Mahadevan L, Tabin CJ (2011) On the growth and form of the gut. Nature 476:57–62
- Shimokawa K, Kimura-Yoshida C, Nagai N, Mukai K, Matsubara K, Watanabe H, Matsuda Y, Mochida K, Matsuo I (2011) Cell surface heparan sulfate chains regulate local reception of FGF signaling in the mouse embryo. Dev Cell 21:252–272
- Sidney LE, Branch MJ, Dunphy SE, Dua HS, Hopkinson A (2014) Concise review: evidence for CD34 as a common marker for diverse progenitors. Stem Cells 32:1380-1389
- Simon-Assmann P, Lefebvre O, Bellissent-Waydelich A, Olsen J, Orian-Rousseau V, Dearcangelis A (1998) The Laminins: role in intestinal morphogenesis and differentiation.

Ann N Y Acad Sci 859:46–64

- Taber LA (2006) Biophysical mechanisms of cardiac looping. Int J Dev Biol 50:323–332
- Chiquet-Ehrismann R, Tucker RP (2011) Tenascins and the importance of adhesion modulation. Cold Spring Harb Perspect Biol 3:a004960
- Welsh IC, Thomsen M, Gludish DW, Alfonso-Parra C, Bai Y, Martin JF, Kurpios NA (2013) Integration of left-right *Pitx2* Transcription and Wnt signaling drives asymmetric gut morphogenesis via Daam2. Dev Cell 26:629–644
- Whiting CV, Tarlton JF, Bailey M, Morgan CL, Bland PW (2003) Abnormal mucosal extracellular matrix deposition is associated with increased TGF-beta receptor-expressing mesenchymal cells in a mouse model of colitis. J Histochem Cytochem 51:1177-1189

Figure legends

Fig. 1 Areas measured for histoplanimetry

a Schema of the mouse duodenojejunal flexure (DJF) section at the pre-formation stage. The areas measured for the inner and outer bending sides of the DJF are indicated in green and blue, respectively. Black line indicates the boundary between the two areas crossing the dorsal and ventral mesenteries.

b Schema of the mouse DJF section at the post-formation stage. Black square indicates the area measured, indicated in green and blue for the inner and outer bending sides of the DJF, respectively. Dotted line indicates the boundary between the outside and inside areas. Epi, mucosal epithelium.

Fig. 2 Comparison of Alcian Blue-positivity between the inner and outer bending sides of the mouse duodenojejunal flexure (DJF)

a and b Alcian Blue staining at pH1.0 with eosin counterstaining in the mouse DJF at the post-formation stage. (**b**) is a high magnification view of (**a**).

c and d Alcian Blue staining at pH2.5 with eosin counterstaining in the mouse DJF at the post-formation stage. (**d**) is a high magnification view of (**c**).

e and f Alcian Blue staining at pH1.0 in the mouse DJF at the pre- (**e**) and post- (**f**) formation stages. Arrowheads, mucosal epithelial basement membrane. Double daggers, intercellular space. Arrows, endothelial basement membrane.

g Comparison of integrated density (IntDen) ratio for the Alcian Blue-positive reactions at pH1.0.

h and i Alcian Blue staining at pH2.5 in the mouse DJF at the pre- (**h**) and post- (**i**) formation stages.

j Comparison of IntDen ratio for Alcian Blue-positivity at pH2.5. Asterisk indicates significant difference between the inner and outer bending sides of the DJF, given by the Wilcoxon test ($P < 0.05$). Values = mean ± standard error; $n \geq 4$. The schema beneath the graph summarizes the difference in the IntDen ratio. Darker blue indicates higher IntDen ratio.

Bars, 50 μm. I, inner side of the DJF. O, outer side of the DJF.

Fig. 3 Comparison of fibronectin- and collagen I-positivity between the inner and outer bending sides of the mouse duodenojejunal flexure (DJF)

a and b Immunohistochemistry for fibronectin in the mouse DJF at the pre- (**a**) and post- (**b**) formation stages. Double daggers, intercellular space. Arrows, mucosal epithelial basement membrane.

c Comparison of IntDen ratios for the fibronectin-positive reactions. The schema beneath the graph summarizes the difference in the IntDen ratio. Darker brown indicates higher IntDen ratio.

d and e Immunohistochemistry for collagen I in the mouse DJF at the pre- (**d**) and post- (**e**) formation stages. Black arrowheads, collagen I-positivity in the intercellular space.

f Comparison of IntDen ratio for collagen I-positivity. Asterisk indicates significant difference between the inner and outer bending sides of the DJF as given by the Wilcoxon test ($P < 0.05$). Values = mean ± standard error; $n \geq 4$. The schema beneath the graph summarizes the difference in the IntDen ratio. Darker brown indicates higher IntDen ratio.

g and h High magnification views of (**e**) at the inner (**g**) and the outer (**h**) bending sides of the DJF. Black arrowheads, scattered collagen I-positive reactions. White arrowheads, assembled collagen I-positive reactions. Bars, 50 μm. I, inner side of the DJF. O, outer side of the DJF.

Fig. 4 Comparison of pan-tenascin-positivity between the inner and outer bending sides of the mouse duodenojejunal flexure (DJF)

a and b Immunohistochemistry for pan-tenascin in the mouse DJF at the pre- (**a**) and post- (**b**) formation stages. Arrowheads indicate pan-tenascin-positivity in the intercellular space close to the mucosal epithelial basement membrane for (**a**) and the outside of the DJF for (**b**).

c Comparison of IntDen ratios for pan-tenascin-positivity. Asterisk indicates significant difference between the inner and outer bending sides of the DJF as given by the Wilcoxon test ($P < 0.05$). Values = mean ± standard error; $n \geq 4$. The schema beneath the graph summarizes the difference in the IntDen ratio. Darker brown indicates higher IntDen ratio.

d and e High magnification views of (**a**) at the inner (**d**) and outer (**e**) bending sides of the DJF. Bars, 50 μm. DM, dorsal mesentery. I, inner side of the DJF. O, outer side of the DJF.

Fig. 5 Comparison of collagen IV-positivity between the inner and outer bending sides of the mouse duodenojejunal flexure (DJF)

a and b Immunohistochemistry for collagen IV in the mouse DJF at the pre- (**a**) and post- (**b**) formation stages.

c Comparison of the IntDen ratio for collagen IV-positivity. The asterisk indicates a significant difference between the inner and outer bending sides of the DJF for the Wilcoxon test ($P < 0.05$). Values = mean ± standard error; $n \geq 4$. The schema beneath the graph summarizes the difference in the IntDen ratio. Darker brown indicates higher IntDen ratio.

d, e, f High magnification views of (**a**) at the inner (**d**) and the outer (**e**) bending sides of the DJF and around the mucosal epithelium (**f**). Epi, mucosal epithelium. Arrowheads, collagen IV-positivity in the mucosal epithelial and endothelial basement membranes. Arrows, collagen

IV-positivity in the mesothelial basement membrane. Bars, 50 μm. I, inner side of the DJF. O, outer side of the DJF.

Fig. 6 Comparison of pan-laminin-positivity between the inner and outer bending sides of the mouse duodenojejunal flexure (DJF)

a Immunohistochemistry for pan-laminin in the mouse DJF at the pre-formation stage.

b and c High magnification views of (**a**) at the inner (**b**) and the outer (**c**) bending sides of the DJF.

d Immunohistochemistry for pan-laminin in the mouse DJF at the post-formation stage.

e and f High magnification views of (**d**) at the inner (**e**) and outer (**f**) bending sides of the DJF.

g High magnification views of (**a**) around the mucosal epithelium.

h Comparison of IntDen ratios for the pan-laminin-positive reactions. Asterisk indicates significant difference between the inner and outer bending sides of the DJF as given by the Wilcoxon test ($P < 0.05$). Values = mean ± standard error; $n \geq 4$. The schema beneath the graph summarizes the difference in the IntDen ratio. Darker brown indicates higher IntDen ratio.

Epi, mucosal epithelium. Arrowheads, pan-laminin-positivity in the mucosal epithelial and endothelial basement membranes. Arrows, pan-laminin-positivity in the mesothelial basement membrane. Bars, 50 μm. I, inner side of the DJF. O, outer side of the DJF.

Fig. 7 Comparison of laminin 1/2-positivity between the inner and outer bending sides of the mouse duodenojejunal flexure (DJF)

a Immunohistochemistry for laminin 1/2 in the mouse DJF at the pre-formation stage.

b and c High magnification views of (**a**) at the inner (**b**) and the outer (**c**) bending sides of the DJF.

d Immunohistochemistry for laminin 1/2 in the mouse DJF at the post-formation stage.

e and f High magnification views of (**d**) at the inner (**e**) and the outer (**f**) bending sides of the DJF. Arrowheads, laminin 1/2-positivity in the mucosal epithelial basement membrane. Arrows, laminin 1/2-positivity in the mesothelial basement membrane.

g Comparison of IntDen ratios for the laminin 1/2-positive reactions. Asterisk indicates significant difference between the inner and outer bending sides of the DJF as given by the Wilcoxon test ($P < 0.05$). Values = mean ± standard error; $n \geq 4$. The schema beneath the graph summarizes the difference in the IntDen ratio. Darker brown indicates higher IntDen ratio.

h Immunofluorescence for N-cadherin in the mouse DJF at the pre-formation stage.

i and j High magnification views of (**h**) at the inner (**j**) and the outer (**i**) bending sides of the DJF.

k Immunofluorescence for N-cadherin in the mouse DJF at the post-formation stage.

l and m High magnification views of (**k**) at the inner (**m**) and the outer (**l**) bending sides of the DJF. Arrowheads, neural crest cells and neurons. Arrows, N-cadherin-positivity in the outside area. Epi, mucosal epithelium. DM, dorsal mesentery. Bars, 50 μm. I, inner side of the DJF. O, outer side of the DJF.

Fig. 8 Schema summarizing distribution of the ECM molecules examined in the mouse duodenojejunal flexure (DJF)

a and b Schemas of histological view of the mouse DJF at the pre- (**a**) and post- (**b**) formation stages. AB, Alcian Blue. Epi, mucosal epithelium. I, inner side of the DJF. Mes, mesenchyme. Meso, mesothelium. O, outer side of the DJF.

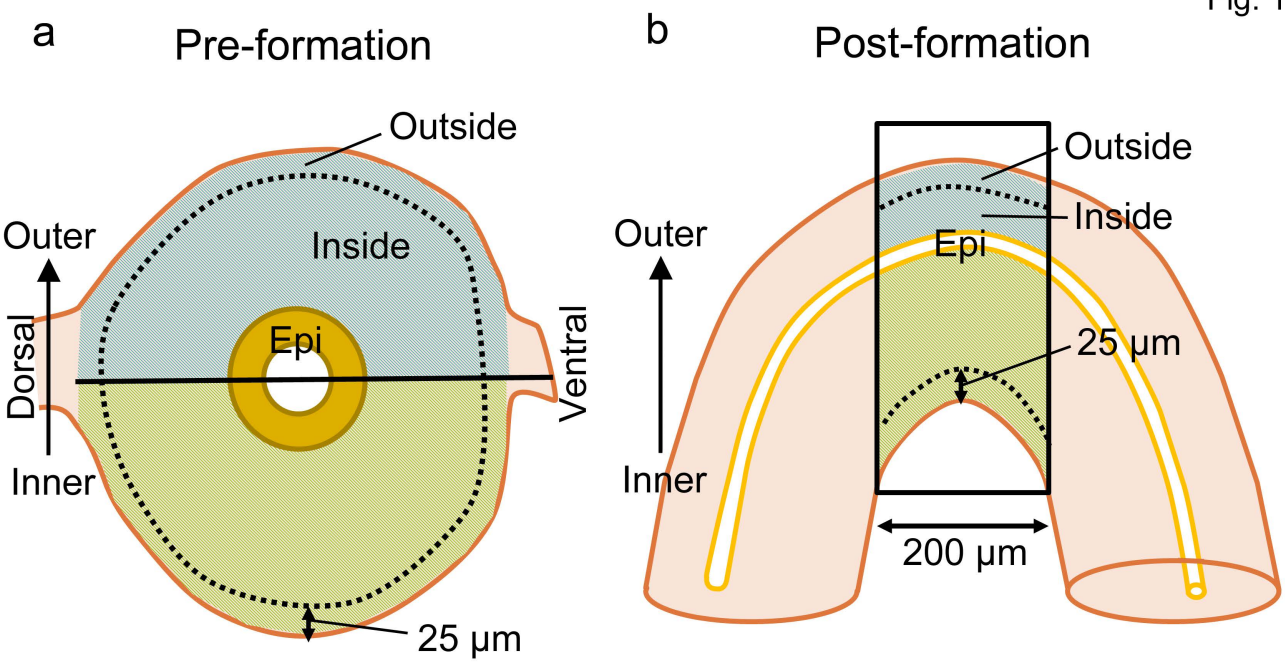
a
Pre-formation
Outside
Outer
Inside
Epi
Dorsal
Ventral
Inner
25 μm
b
Post-formation
Outside
Inside
Outer
Epi
25 μm
Inner
200 μm

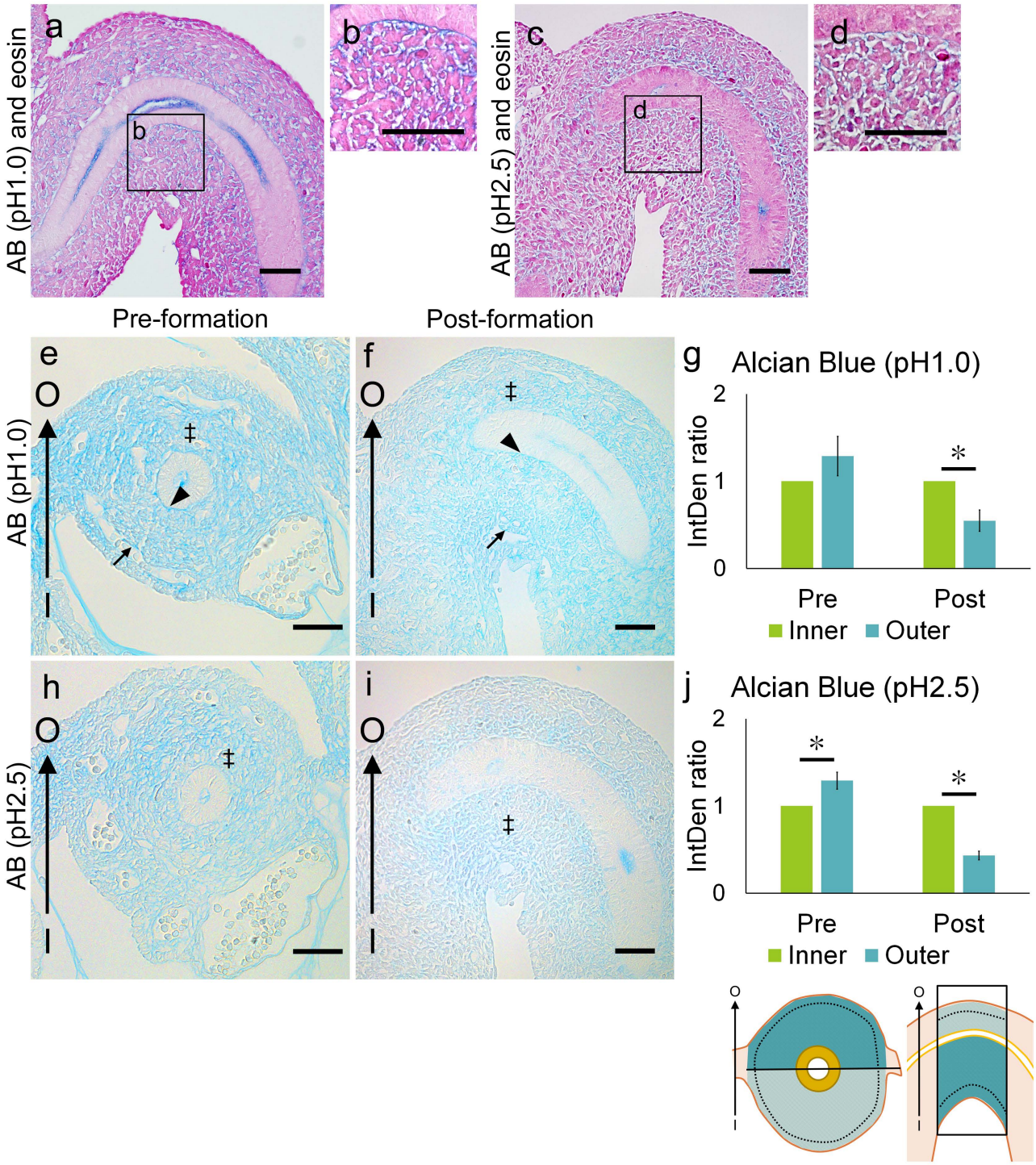
a
b
c
d
AB (pH1.0) and eosin
AB (pH2.5) and eosin
Pre-formation
Post-formation
e
f
g
Alcian Blue (pH1.0)
AB (pH1.0)
IntDen ratio
2
1
0
*
Pre
Post
Inner
Outer
h
i
j
Alcian Blue (pH2.5)
AB (pH2.5)
O
I
‡

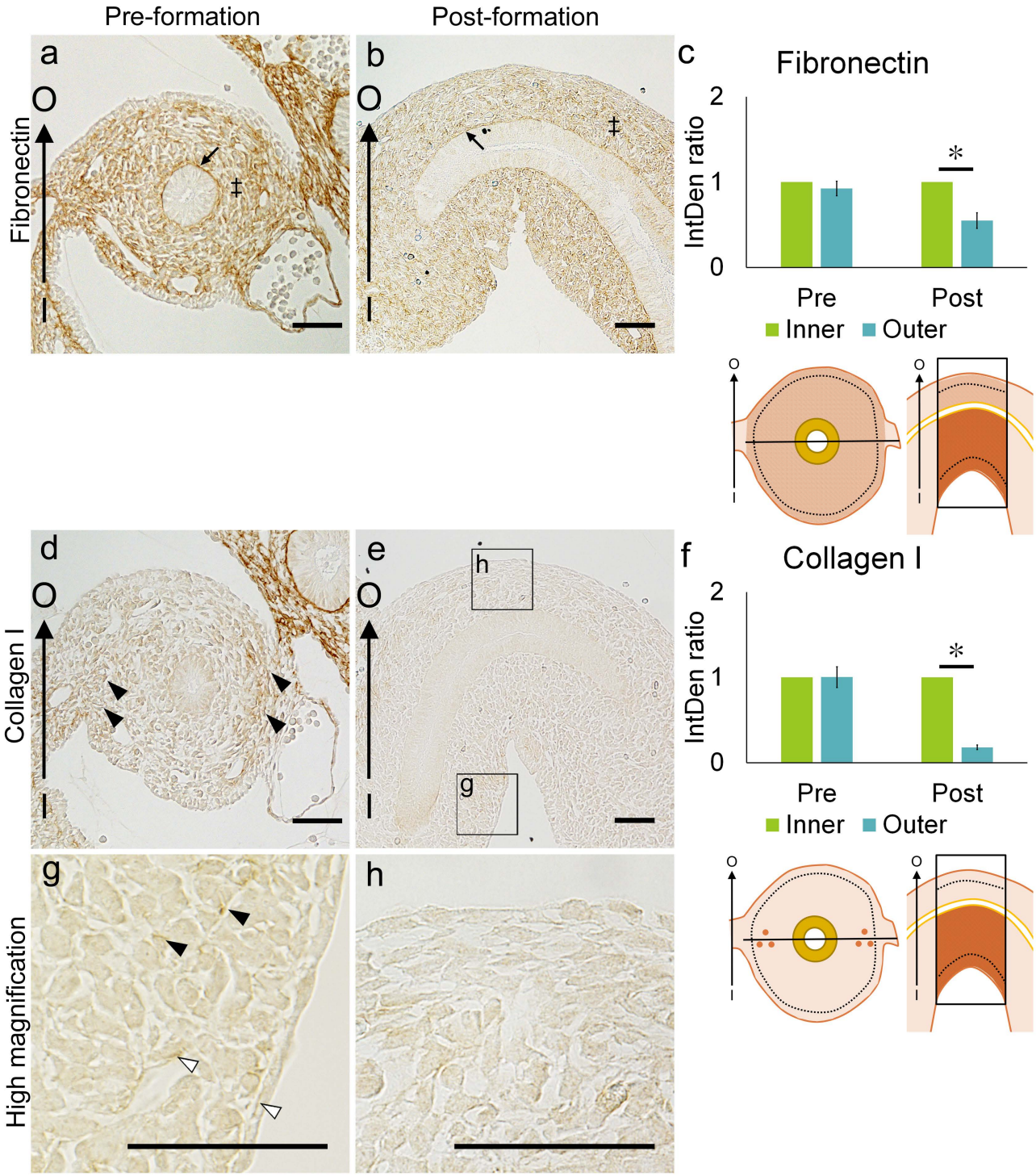
Pre-formation
Post-formation
a
b
c
Fibronectin
O
I
‡
IntDen ratio
2
1
0
*
Pre
Post
Inner
Outer
d
e
f
Collagen I
h
g
High magnification

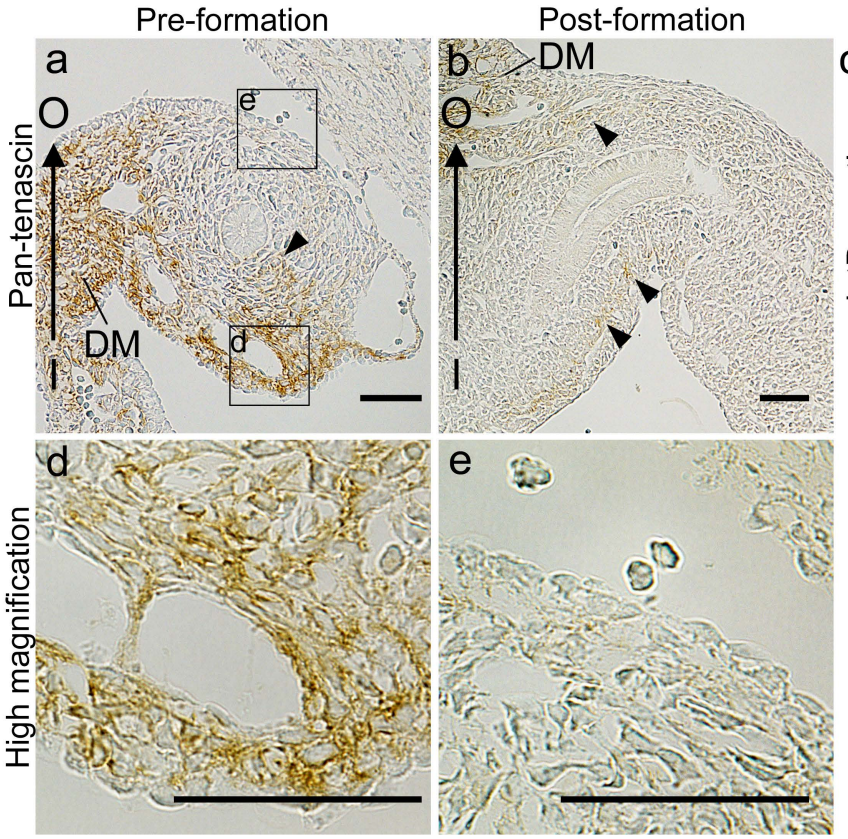
Pre-formation
Post-formation
a
b
c
d
e
O
I
DM
Pan-tenascin
High magnification
Pan-tenascin
IntDen ratio
3
2
1
0
*
Pre
Post
Inner
Outer

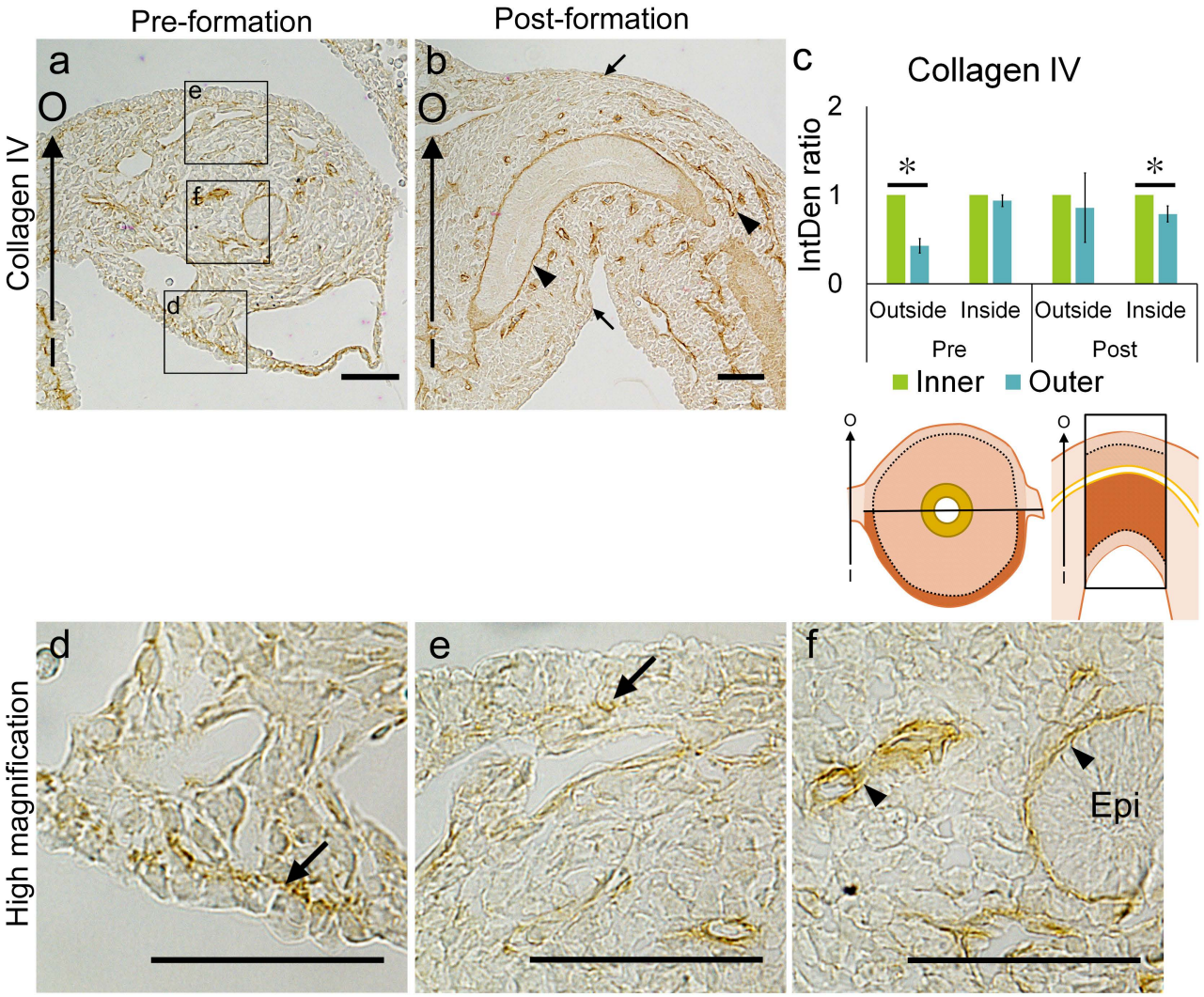
Pre-formation
Post-formation
a
b
c
Collagen IV
O
e
f
d
Collagen IV
IntDen ratio
2
1
0
*
*
Outside
Inside
Outside
Inside
Pre
Post
Inner
Outer
High magnification
d
e
f
Epi

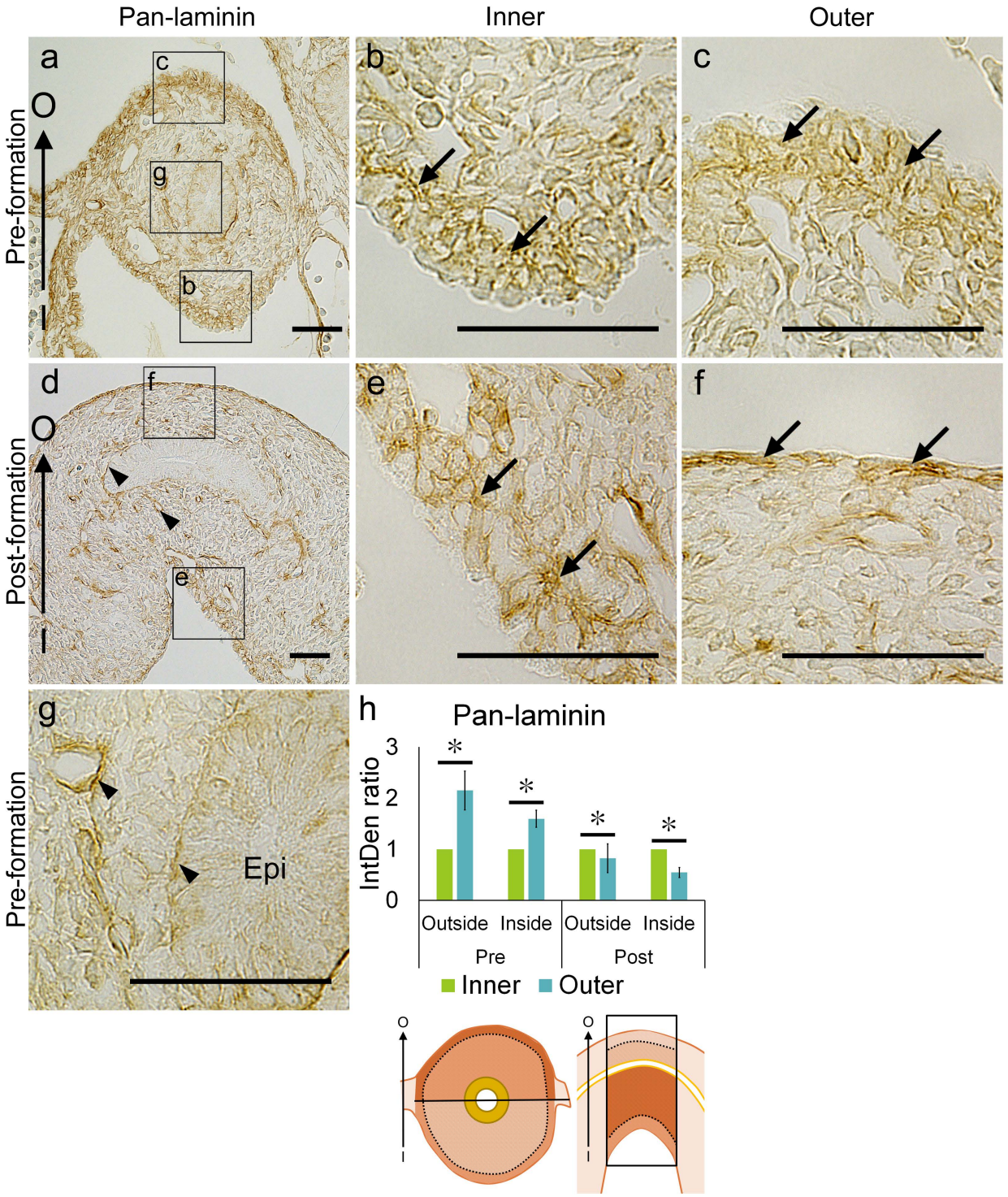
Pan-laminin
Inner
Outer
a
b
c
d
e
f
g
h
Pre-formation
Post-formation
O
I
Epi
Pan-laminin
IntDen ratio
3
2
1
0
*
Outside
Inside
Outside
Inside
Pre
Post
Inner
Outer

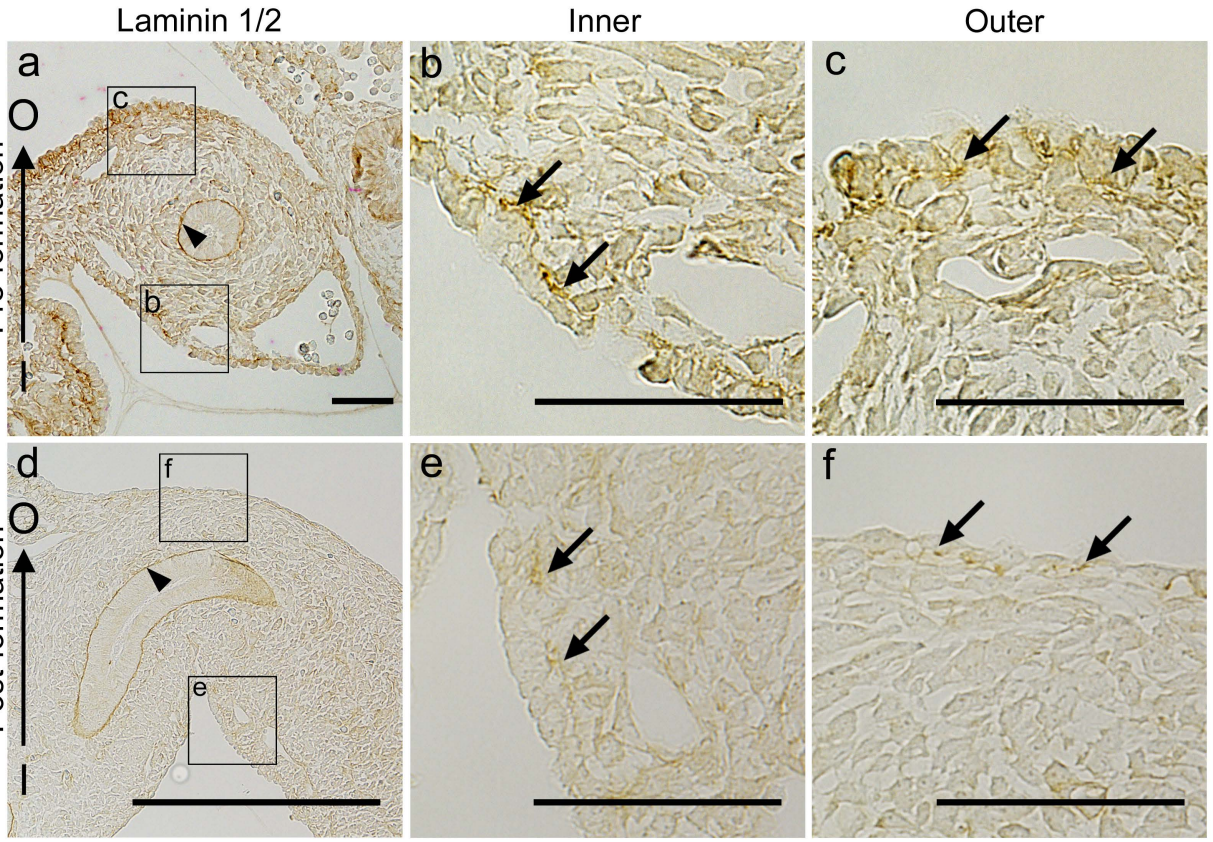
Laminin 1/2
Inner
Outer
a
b
c
d
e
f
O
I
Pre-formation
Post-formation

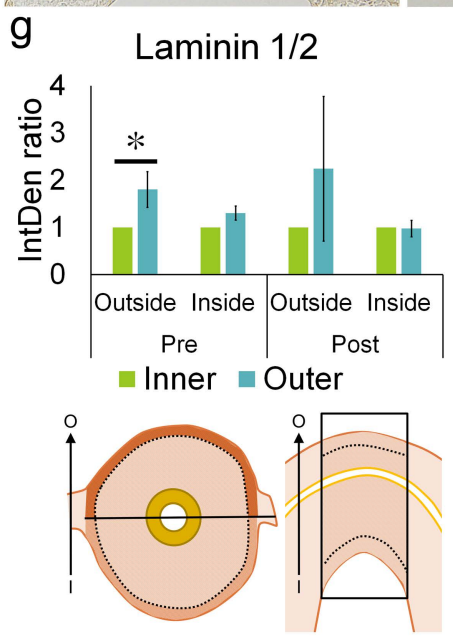
g
Laminin 1/2
IntDen ratio
4
3
2
1
0
*
Outside
Inside
Outside
Inside
Pre
Post
Inner
Outer
O
I

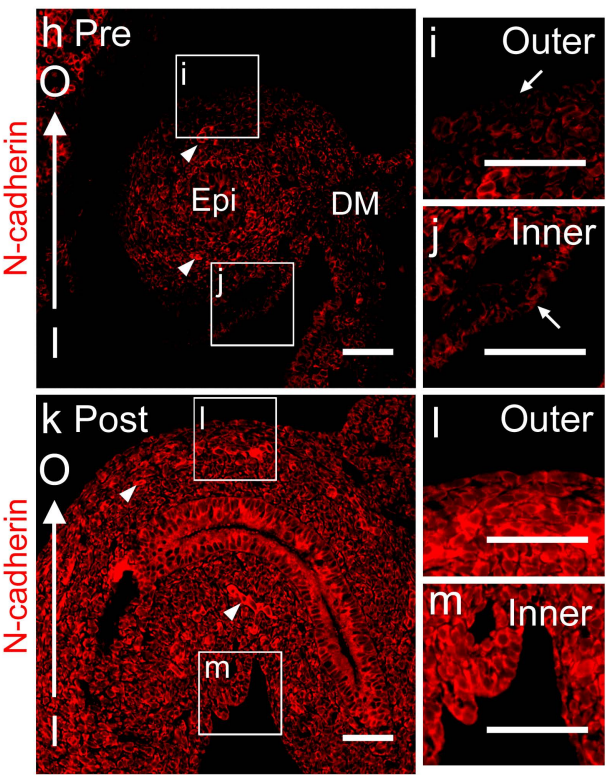
h Pre
i
j
Epi
DM
N-cadherin
O
I
Outer
Inner
k Post
l
m
Outer
Inner

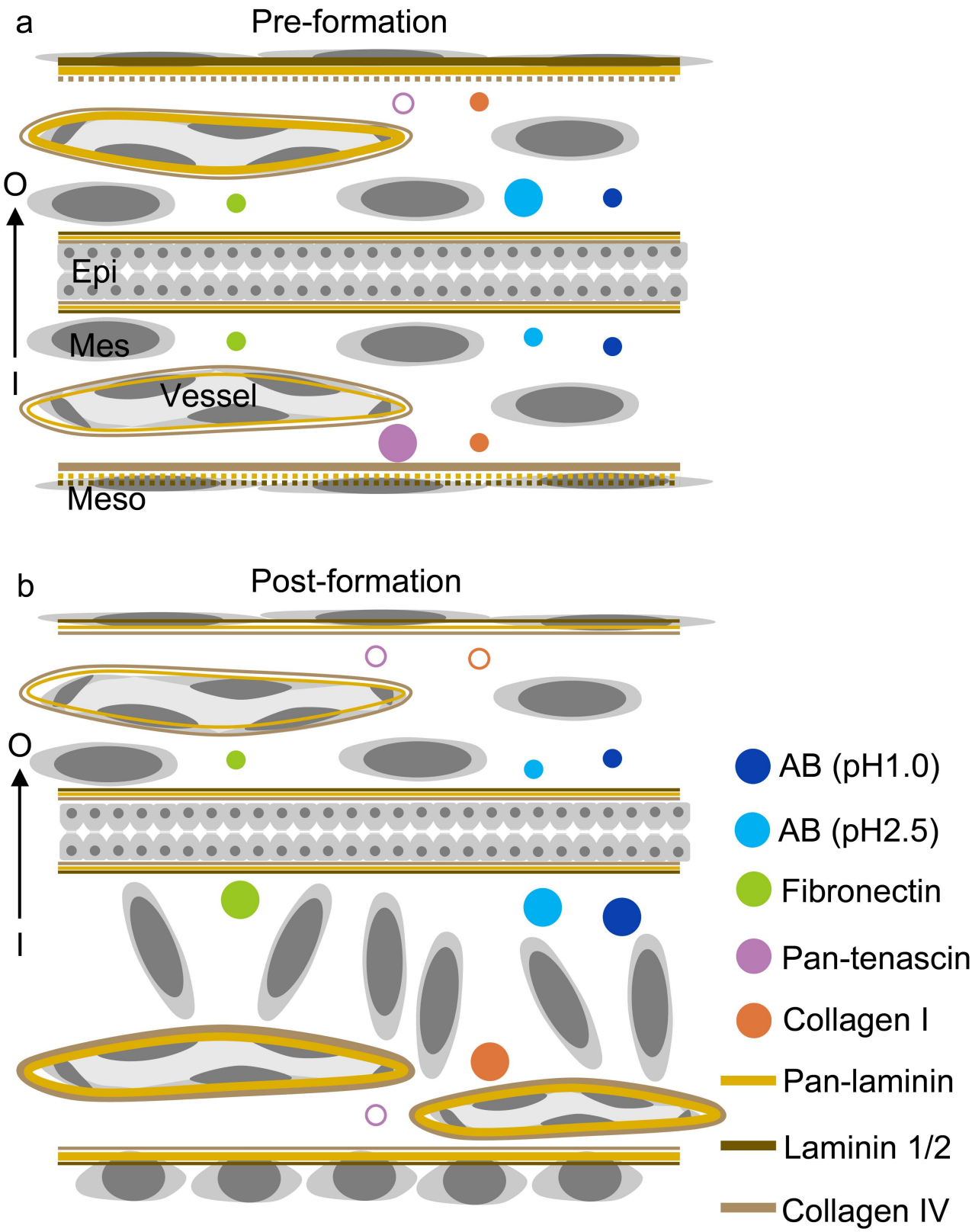
a
Pre-formation
O
I
Epi
Mes
Vessel
Meso
b
Post-formation
O
I
AB (pH1.0)
AB (pH2.5)
Fibronectin
Pan-tenascin
Collagen I
Pan-laminin
Laminin 1/2
Collagen IV